Journal of Controlled Release 157 (2012) 366–374

Contents lists available at SciVerse ScienceDirect

Journal of Controlled Release

journal homepage: www.elsevier.com/locate/jconrel

Influence of formulation variables on the biodistribution of multifunctional block copolymer micelles

Humphrey Fonge [a], Huang Huang [a], Deborah Scollard [a], Raymond M. Reilly [a,b,c], Christine Allen [a,d,e,*]

[a] Leslie Dan Faculty of Pharmacy, University of Toronto, Toronto, ON, Canada
[b] Department of Medical Imaging, University of Toronto, Toronto, ON, Canada
[c] Toronto General Research Institute, University Health Network, Toronto, ON, Canada
[d] Department of Chemistry, University of Toronto, Toronto, ON, Canada
[e] STTARR Innovation Centre, Radiation Medicine Program, Princess Margaret Hospital, University Health Network, Toronto, ON, Canada

ARTICLE INFO

Article history:
Received 3 May 2011
Accepted 22 September 2011
Available online 1 October 2011

Keywords:
Pharmacokinetics
Block copolymer micelles (BCMs)
Bifunctional chelators (BFCs)
Indium-111
Human epidermal growth factor (hEGF)

ABSTRACT

The physico-chemical characteristics and composition of block copolymer micelles (BCMs) may influence the pharmacokinetics and consequently, the desired delivery characteristics. In this study the influence of formulation variables such as size, density of targeting ligand [i.e. epidermal growth factor (hEGF)] and the bifunctional chelator (BFC) used for labelling the BCMs with ^{111}In, on the pharmacokinetics and biodistribution in mice were evaluated. BCMs were prepared from Me-PEG$_x$-*b*-PCL$_y$ ($x = 2.5$ k, $y = 1.2$ k for 15 nm BCMs and $x = 5$ k, $y = 5$ k for 60 nm BCMs) with (targeted, 1 or 5 mol% hEGF) or without (non-targeted) hEGF-PEG$_x$-*b*-PCL$_y$. To investigate the effect of the BFC on the pharmacokinetics, the BCMs were labelled with ^{111}In using *p*-SCN-Bn-DOTA (Bn-DOTA-PEG$_x$-*b*-PCL$_y$), H_2N-DOTA (DOTA-PEG$_x$-*b*-PCL$_y$), DTPA anhydride (DTPA-PEG$_x$-*b*-PCL$_y$) or *p*-SCN-Bn-DTPA (Bn-DTPA-PEG$_x$-*b*-PCL$_y$). The resulting 15 nm or 60 nm non-targeted or targeted (1 or 5 mol% hEGF) were injected via a tail vein to mice bearing MDA-MB-468 human breast cancer xenograft that overexpress EGFR, followed by pharmacokinetics and biodistribution studies. Pharmacokinetic parameters were determined by fitting the blood concentration vs time data using a two compartment model with i.v. bolus input. Pharmacokinetic parameters were found to depend on BCM size, the BFC used as well as the density of hEGF on the surface of the BCMs. BCMs labelled with *p*-SCN-Bn-DTPA (^{111}In-Bn-BCMs) showed improved pharmacokinetics (i.e. extended circulation lifetime) and tumor uptake compared to those labelled with DOTA-PEG$_x$-*b*-PCL$_y$, *p*-SCN-Bn-DOTA or DTPA dianhydride. Formulations with a high density of hEGF (5 mol% hEGF) had short circulation half-lives. BCMs labelled with ^{111}In via *p*-SCN-Bn-DTPA showed highest accumulation in the liver and spleen and slower whole body elimination. Smaller sized BCMs were rapidly cleared from the circulation. Increasing the density of hEGF on the surface did not improve tumor uptake due to faster clearance from the circulation. To achieve improved pharmacokinetics and in turn effective exploitation of the EPR effect, *p*-SCN-Bn-DTPA emerged as the optimal BFC for radiolabelling BCMs while a lower density of hEGF gave more favourable organ distribution.

1. Introduction

In recent years, drugs relying on formulations in nanotechnologies such as Doxil®/Myocet® and Fungisome/AmBisome have been approved for clinical use [1–3], while many others have reached late stage clinical development [4–7]. The promise of nanotechnologies in drug delivery relies on their ability to significantly increase the payload of therapeutic agents that reach a diseased site while limiting systemic toxicity [8–10]. Additionally, these nanoparticles when labelled with radionuclides [11,12] and/or contrast agents can be used for imaging, contrast enhancement [13,14] and/or as radiotherapeutics.

Efficient targeting using nano-delivery systems relies largely on passive targeting which is achieved via exploitation of the enhanced permeation and retention (EPR) effect. The size of nanoparticles and presence of steric stabilizing polymers such as poly(ethylene glycol) (PEG) at their surface facilitates retention within the circulation for extended periods following intravenous (i.v.) administration. This prolonged circulation lifetime for the nanoparticles is essential for passive targeting to tumors which have leaky vasculature, via the EPR effect. In addition to the physico-chemical characteristics of nanoparticles (i.e. size, surface properties), the tumor microenvironment is also responsible for determining the extent of extravasation of these nanoparticles into tumors [15].

* Corresponding author at: Department of Pharmaceutical Sciences, University of Toronto 144 College Street, Toronto, ON, Canada M5S 3M2. Tel.: +1 416 946 8594; fax: +1 416 978 8511.
E-mail address: cj.allen@utoronto.ca (C. Allen).

0168-3659/$ – see front matter © 2011 Elsevier B.V. All rights reserved.
doi:10.1016/j.jconrel.2011.09.088

Active targeting may also be pursued as a strategy to improve the efficacy of drug formulations. Active targeting requires the surface conjugation of targeting moieties that are specific for receptors selectively present or overexpressed at a diseased site. Indeed numerous preclinical studies have demonstrated that active targeting of nanoparticle-based formulations can result in improvements in efficacy in comparison to the non-targeted formulations [16–18]. However, the relationship between the therapeutic effect of the actively targeted nanoparticles and distribution at the whole body, tumor and cellular levels is less clear. Overall, it is critical that the addition of the targeting moiety does not result in a reduction in the circulation lifetime of the nanoparticle and in turn a decrease in tumor accumulation via the EPR effect and efficacy [19,20].

The pharmacokinetics of nano-delivery systems depends on their surface properties, size and morphology [21–26]. Based on the present literature it is debateable whether or not the presence (and therefore the density) of targeting moieties at the surface of vehicles influences their pharmacokinetic properties. Some studies have shown that incorporation of targeting moieties leads to a reduction in circulation lifetime while others show no such difference in comparison to the non-targeted delivery systems [16,17,27]. However, in the case of immunoliposomes conjugated using whole IgG there is consensus that the Fc mediated clearance and increased opsonisation of the antibody labelled vehicles leads to poorer pharmacokinetics [27]. While the increased opsonisation has been well documented in some cases for nano-delivery systems conjugated with antibodies or antibody fragments, few studies have examined such effects for small ligands [< 10 kDa, e.g. epidermal growth factor (EGF)]. As well, given the recent interest in image-guided drug delivery and molecular imaging, delivery systems are frequently being labelled with radionuclides via use of a bifunctional chelating (BFC) agent. As has been shown with some proteins (e.g. affibodies conjugated with DOTA or DTPA derivatives) the use of BFC agents can have a profound influence on the pharmacokinetics of biomolecules [28–31]. However, the effects of such BFC agents on the pharmacokinetics and biodistribution of nano-delivery systems have not been studied in detail.

Our group is exploring the use of BCMs for the treatment and diagnosis of EGFR overexpressing cancers [11,12,32]. As shown in Fig. 1, the BCMs consist of a stabilizing methoxypoly(ethylene glycol)-block-polycaprolactone copolymer (MePEG-*b*-PCL), an ^{111}In radionuclide carrying PEG-*b*-PCL copolymer and a targeting component hEGF-PEG-*b*-PCL. In the current study, the influence of several formulation variables (i.e. BCM size, density of EGF and BFC agent selected) on the pharmacokinetics and biodistribution of the actively targeted micelles were examined in order to maximize their delivery to the target site.

2. Materials and methods

2.1. Materials

$MePEG_x$ ($x = 2.5$ k, and $x = 5$ k, polydispersity index (PDI) = 1.06) obtained from Sigma-Aldrich (St. Louis, MO) and NH_2PEG_x ($x = 2.5$ k, and $x = 5$ k, PDI = 1.07) obtained from JenKem Technology (Allen, TX), were dried twice by azeodistillation in toluene. ε-Caprolactone (CL, 99%) was obtained from Sigma-Aldrich and dried with *n*-butyl lithium (at −78 °C), calcium hydride and molecular sieves, prior to use. Tetrahydrofuran (THF, 99.9%) and toluene (99.9%) were obtained from Sigma-Aldrich and were refluxed over a sodium–benzophenone complex and distilled under nitrogen. HCl (1.0 M in diethyl ether), sodium (99.5%), and diethylenetriaminetetraacetic acid dianhydride (DTPA dianhydride) were obtained from Sigma-Aldrich. 2-(4-thiocyanatobenzyl)-1,4,7,10-tetraazacyclododecane-1,4,7,10-tetraacetic acid (*p*-SCN-Bn-DOTA), 1,4,7.10-Tetraazacyclododecane-1,4,7,10-tetraacetic acid mono(1-hydroxysucinimide ester) (DOTA-NHS-ester) and 2-(4-isothiocyanatobenzyl)-diethylenetriaminepentaacetic acid (*p*-SCN-Bn-DTPA) were obtained from Macrocyclics (Dallas TX). hEGF was obtained from Meridian Life Sciences (Memphis, TN). $^{111}InCl_3$ was purchased from Nordion (Kanata, ON).

2.2. Synthesis and characterization of MePEG-b-PCL, NH_2-PEG-b-PCL and HOOC-PEG-b-PCL

Carboxy-terminated poly(ethylene glycol)-*b*-poly(ε-caprolactone) (HOOC-PEG_x-*b*-PCL_y), methoxy-terminated PEG_x-*b*-PCL_y ($MePEG_x$-*b*-PCL_y) and amino-terminated PEG_x-*b*-PCL_y (H_2N-PEG_x-*b*-PCL_y) copolymers were prepared as previously reported [32–34]. N-hydroxysuccinimidyl PEG_x-*b*-PCL_y activated ester (NHS-PEG_x-*b*-PCL_y) and hEGF-PEG_x-*b*-PCL_y were synthesized as previously described [34]. The conjugation efficiency (and the amount of hEGF conjugated to BCMs) was determined by the μBCA assay (Pierce Scientific) following the manufacturer's guidelines.

DTPA derivatization of H_2N-PEG_x-*b*-PCL_y was accomplished using DTPA bis-anhydride or *p*-SCN-Bn-DTPA and was purified as previously described [11,32]. DOTA-PEG_x-*b*-PCL_y and Bn-DOTA-PEG_x-*b*-PCL_y were obtained following the similar procedure as for the DTPA derivatives.

Block copolymers (in $CDCl_3$) were characterized by ^{1}H NMR using a Gemini 200 spectrometer (200 MHz for ^{1}H). The molecular weights of polymers were determined by analyzing the ratio of the proton intensities in the ^{1}H-NMR spectra. Gel permeation chromatography (GPC) measurements to determine the molecular weight and PDI of the polymers were carried out at 40 °C using a Waters 2695 liquid chromatography system equipped with three Waters Styragel HR 4E columns (10 μm, 7.8 × 300 mm) connected in series (Waters Inc.; Mississauga, ON). The column effluent was connected to a refractive index detector (Waters Inc., Mississauga, ON) which was previously calibrated using polystyrene standards (Polysciences Inc.; Warrington, PA). THF with 1% triethylamine was used as mobile phase at a flow rate of 1.0 mL/min at 40 °C. The data were analyzed using Empower software (Waters Inc.; Mississauga, ON). The critical micelle concentration (CMC) of the copolymer was determined using an established method with 1,6-diphenyl-1,3,5-hexatriene (DPH) as the fluorescent probe [35].

2.3. Preparation of ^{111}In-labelled block copolymers

DTPA/Bn-DTPA-conjugated PEG_x-*b*-PCL_y, or DOTA/Bn-DOTA-conjugated PEG_x-*b*-PCL_y (10–25 μg) were radiolabelled with ^{111}In-acetate ($^{111}InCl_3$/sodium acetate, 37–100 MBq) via incubation at pH 6.0 for 30 min. Purity of the complex was determined on Whatman ITLC-SG strips (Pall Life Sciences; St. Laurent, QC, Canada) developed in 100 mM sodium citrate pH 5.0. ^{111}In-labelled block copolymers remained at the origin ($R_f = 0$) while free ^{111}In-DTPA/^{111}In-acetate migrated with the solvent front ($R_f = 1$). A radiochemical purity of 96–98% was achieved.

2.4. Preparation of ^{111}In-labelled block copolymer micelles

$MePEG_x$-*b*-PCL_y micelles (BCMs) were prepared by the "dry down" method as previously described [11]. Briefly, 60 nm or 15 nm BCMs were prepared by dissolving 50 mg of $MePEG_{5k}$-*b*-PCL_{5k} or $MePEG_{2.5\text{-}k}$-*b*-$PCL_{1.2k}$, respectively, in 1 mL DMF and stirring for 4 h, after which the solution was dried under an atmosphere of N_2 and reduced pressure in a vacuum overnight. The resulting dry film was then hydrated with 1 mL of filtered Milli-Q water at 60 °C with vortexing. The hydrated micelle solution was then stirred at room temperature for 48 h followed by 1 h sonication at room temperature. The hydrodynamic diameters of BCMs were determined by dynamic light scattering (DLS) at an angle of 90° at room temperature (90Plus Particle Size Analyzer; Brookhaven Instruments Corp.; Holtsville, NY). Sample solutions of 1–20 mg/mL BCMs were prepared from the stock and

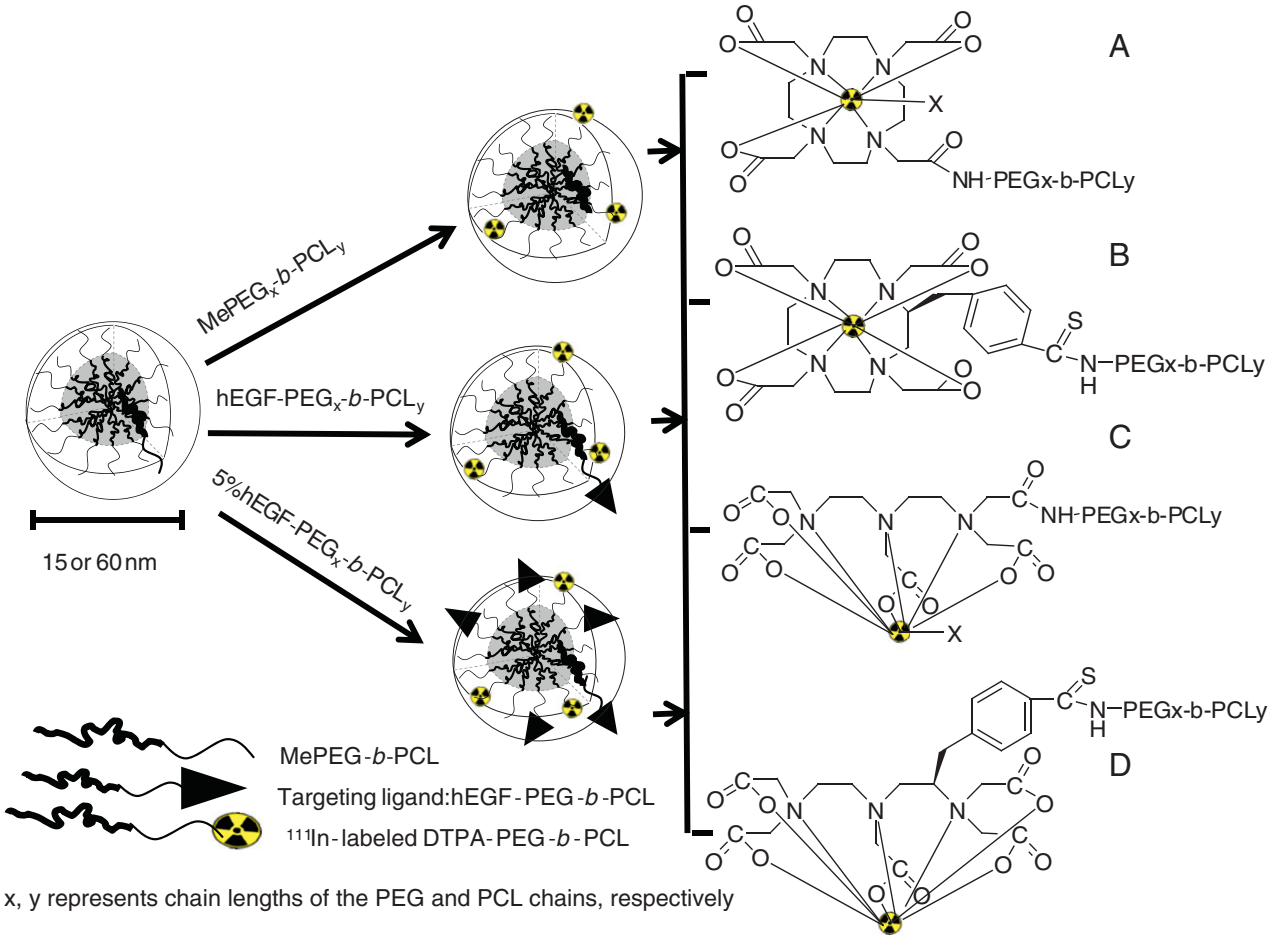

Fig. 1. Physicochemical composition of the different block copolymer micelles (BCMs) formulations. 60 nm non-targeted BCMs radiolabelled with ^{111}In via A) DOTA chelator (^{111}In-DOTA-BCMs) or B) *p*-SCN-Bn-DOTA (^{111}In-Bn-DOTA-BCMs), or C) 15 nm/60 nm targeted (1 mol% hEGF) or non-targeted BCMs labelled with ^{111}In via DTPA bis-anhydride (15 nm/60 nm ^{111}In-BCMs or ^{111}In-hEGF-BCMs) or D) 15 nm/60 nm targeted (5 mol%, hEGF) or non-targeted BCMs labelled with ^{111}In via a *p*-SCN-Bn-DTPA.

analyzed by DLS. BCM morphology was evaluated by transmission electron microscopy (TEM) with a Hitachi 7000 microscope operating at an acceleration voltage of 75 kV (Schaumburg, IL) and the TEM images were analyzed using SigmaScan Pro software (Jandel Scientific).

15 nm and 60 nm ^{111}In-labelled BCMs were prepared by incorporating the ^{111}In-labelled block copolymer with (targeted) or without (non-targeted) hEGF-PEG$_x$-*b*-PCL$_y$ (at a concentration of 1 mol% or 5 mol% hEGF) into the preformed BCMs at 60 °C followed by stirring overnight (Fig. 1).

Incorporation of the ^{111}In-labelled block copolymer into preformed BCMs was verified by Superose 12 Gel filtration flash chromatography using PBS as mobile phase at a flow rate of 0.25 mL/min. Column eluate was collected over 30 min and radioactivity was measured using a γ-counter (Wizard Model 1480, Perkin Elmer, Turku, Finland) [36].

2.5. Cell culture and tumor xenograft model

MDA-MB-468 (1×10^6 EGFR/cell) [37] BC cells were purchased from the American Type Culture Collection (Manassas, VA). The cells were cultured at 37 °C and 5% CO_2 in RPMI 1640 medium containing 1% penicillin–streptomycin solution (1000 U/mL, Invitrogen, Grand Island, NY) and supplemented with 10% fetal bovine serum (FBS, Invitrogen, Grand Island, NY). Sub-confluent cells were harvested by trypsinization with trypsin-EDTA (Sigma Aldrich, Mississauga, ON).

All aspects of animal experiments and husbandry were carried out in compliance with Canadian Council on Animal Care regulations and were approved by the Animal Care Committee of the University of Toronto (protocol #989.3). 4–6 week-old female athymic CD-1 nude mice (18–25 g) were implanted subcutaneously with 1.5×10^7 MDA-MB-468 cells suspended in saline. Tumors were allowed to grow until they reached a diameter of 5–10 mm (3–4 weeks post implantation) prior to administration of the BCM formulations.

2.6. Evaluation of pharmacokinetics and biodistribution in tumor bearing mice

Tumor bearing mice ($n=4$ per group) were injected intravenously via the tail vein with 15 nm non-targeted BCMs (^{111}In-BCMs or ^{111}In-Bn-BCMs), 15 nm hEGF-BCMs (1 mol% or 5 mol% hEGF; ^{111}In-hEGF-BCMs or ^{111}In-Bn-hEGF-BCMs), 60 nm non-targeted BCMs (^{111}In-BCMs, ^{111}In-Bn-BCMs, ^{111}In-DOTA-BCMs, ^{111}In-Bn-DOTA-BCMs), or 60 nm hEGF-BCMs (1 mol% or 5 mol% hEGF; ^{111}In-hEGF-BCMs or ^{111}In-Bn-hEGF-BCMs) at a dose of 250 mg copolymer/kg (5–7 MBq/mouse). Blood samples were collected via the saphenous vein at different time points (5 min to 48 h) using a heparinized capillary tube. The length of the capillary tube occupied by blood was measured using a digital calliper. The amount of blood in the capillary tube was converted to μL using×0.93333 (1 mm of capillary tube occupies 0.93333 μL of blood) as the conversion factor. Radioactivity in the blood was measured in a γ-counter and expressed as a percentage of the injected dose per gram (%ID/g) assuming blood constitutes 7% of the total body weight. Pharmacokinetic parameters were calculated by fitting the blood radiopharmaceutical concentrations to a two-compartment model using Scientist® Ver. 3.0 (Micromath®, Saint Louis, MO). The area under the blood radiopharmaceutical concentration

versus time curves (AUC) were calculated using the trapezoidal rule. Clearance (CL) and volume of distribution at steady state (V_{ss}) were also calculated.

For biodistribution studies, the animals were sacrificed under anaesthesia (Ketamine.HCl (Ketalar®)/Xylazine (Rumpun®)/acepromazine) by cardiac puncture and tissue samples including heart, lung, liver, kidneys, spleen, and tumors were harvested at 48 h.p.i. The tissues were weighed and the amounts of radioactivity in the blood and tissue samples were measured using a γ-counter. Radioactivity in the organs was expressed as %ID/organ and %ID/g organ.

2.7. Statistical analysis

All data were expressed as the mean ± standard deviation (SD) of at least 3 independent experiments. Statistical significance was assessed using a two-tailed Student's *t*-test with $P<0.05$ considered to be significant. All graphs were generated using GraphPad Prism (version 4.03; GraphPad, La Jolla, CA).

3. Results

3.1. Synthesis and characterization of block copolymer micelles

Table 1 shows the characteristics of some of the block copolymers used in this study. Conjugation of the BFC to the amino-terminated block copolymer was achieved with a yield of 40–70%. DLS analyses revealed that the mean diameters of the preformed BCMs were unaffected by the incorporation of the chelating copolymer (DTPA-PEG_x-*b*-PCL_y or DOTA-PEG_x-*b*-PCL_y) and the targeting copolymer (hEGF-$PEG_{2.5k}$-*b*-$PCL_{1.2k}$ or hEGF-PEG_{5k}-*b*-PCL_{5k}). The mean diameters were 15 ± 0.8 nm and 60 ± 1 nm for the Me-$PEG_{2.5k}$-$PCL_{1.2k}$ and Me-PEG_{5k}-PCL_{5k}, BCMs respectively, with monomodal size distributions. As shown in Fig. 2A, BCMs formed from the MePEG_{5k}-*b*-PCL_{5k} copolymer largely had a spherical morphology while Me$PEG_{2.5k}$-*b*-$PCL_{1.2k}$ were spherical with some copolymer forming rod-like structures (Fig. 2B).

To confirm the incorporation of the targeting ligand and the radiolabel into the preformed BCMs, Sepharose 12 gel chromatography with radioactivity detection was used. Fig. 2C shows a representative chromatogram of ^{111}In-Bn-DTPA-PEG_{5k}-*b*-PCL_{5k} (A) and the corresponding (60 nm) ^{111}In-Bn-BCMs (B). In Fig. 2C, the peak at retention time (t_R) 7 min represents the BCMs while the unimers eluted at $t_R = 12$ min.

3.2. Influence of BFCs and concentration of EGF on the pharmacokinetics of block copolymer micelles

Pharmacokinetic parameters CL (mL/h), AUC (%ID/mL × h), V_1 (mL), $t_{1/2\alpha}$ (h) and $t_{1/2\beta}$ (h) were obtained by fitting the blood concentration vs time data using a two-compartment model. Figs. 3 and 4 show the blood clearance curves obtained for the different formulations and for ^{111}In-hEGF. Tables 2 and 3 show the pharmacokinetic parameters of the different ^{111}In-labelled BCM formulations and ^{111}In-hEGF in athymic CD-1 mice bearing MDA-MB-468 tumor xenografts. The distribution half-lives ($t_{1/2\alpha}$) were similar but the elimination half-lives ($t_{1/2\beta}$) varied depending on the size, BFC used and the concentration of EGF on the surface. Similarly, the CL, AUC and V_1 depended on the size, BFC and the concentration of hEGF on the surface.

The nature of the BFC agent conjugated to the micelles and used for radiolabelling was found to have a significant influence on the pharmacokinetics of the BCMs. Fig. 3A and B shows the blood clearance curves and Table 2 shows the pharmacokinetic parameters obtained for the 60 nm BCMs. When BCMs were radiolabelled with ^{111}In via DTPA-anhydride (^{111}In-BCMs) as the BFC, the elimination from the blood was significantly faster than when *p*-SCN-Bn-DTPA (^{111}In-Bn-BCMs) was used. There was no significant difference in $t_{1/2\alpha}$ for ^{111}In-Bn-BCMs (0.6 ± 0.5 h) and ^{111}In-BCMs (0.5 ± 0.2 h) but $t_{1/2\beta}$ of ^{111}In-Bn-BCMs (24.8 ± 7.1 h) was significantly longer ($P=0.006$) than that for ^{111}In-BCMs (11.8 ± 3.3 h). The AUC for ^{111}In-Bn-BCMs (15.6 ± 5.3%ID/mL × h) was 4.6-fold ($P=0.0043$) greater than the AUC for ^{111}In-BCMs (3.4 ± 1.4%ID/mL × h). This resulted in a corresponding decrease in CL ($P=0.0001$) for ^{111}In-Bn-BCMs (0.07 ± 0.02 mL/h) compared to ^{111}In-BCMs (0.3 ± 0.1 mL/h). Similarly, V_1 for ^{111}In-Bn-BCMs (1.5 ± 0.3 mL) was significantly lower ($P=0.006$) than for ^{111}In-BCMs (3.1 ± 0.7 mL).

To further investigate the influence of the BFC agent on the pharmacokinetics of BCMs the micelles were conjugated with NHS-DOTA and *p*-SCN-Bn-DOTA. The pharmacokinetic parameters for these formulations are shown in Fig. 3B and in Table 2. There was no significant difference between $t_{1/2\alpha}$ and $t_{1/2\beta}$ values obtained for the ^{111}In-DOTA-BCMs and the ^{111}In-Bn-DOTA-BCMs. However, CL of ^{111}In-Bn-DOTA-BCMs was significantly lower ($P<0.05$) and the AUC ($P<0.05$) was significantly larger than for ^{111}In-DOTA-BCMs.

Loading hEGF on the surface of preformed ^{111}In-BCMs resulted in a less favourable pharmacokinetic profile characterized by a faster elimination from the circulation. As shown in Table 2, when the concentration of hEGF on the surface of BCMs was 5 mol% (^{111}In-5%hEGF-Bn-BCMs), the CL ($P=0.0001$) and AUC ($P=0.005$) were 15.7-fold (1.1 ± 0.1 mL/h) greater and 2.4-fold (6.6 ± 0.9% ID/mL × h) smaller, respectively, than the corresponding non-targeted ^{111}In-Bn-BCMs (CL: 0.07 ± 0.03 mL/h and AUC: 15.6 ± 5.3 5%ID/mL × h). $t_{1/2\beta}$ of ^{111}In-5%hEGF-Bn-BCMs (15.0 ± 9.1 h) was lower than that for ^{111}In-Bn-BCMs (24.8 ± 7.1 h). Similarly, V_1 for ^{111}In-Bn-BCMs (1.5 ± 0.3 mL) was lower than ^{111}In-5%hEGF-Bn-BCMs (5.1 ± 1.5 mL).

Fig. 4 and Table 3 show the elimination from the blood curve and the pharmacokinetics parameters for the 15 nm BCMs in athymic CD-1 nude mice bearing MDA-MB-468 tumor xenografts. For the 15 nm BCMs, the pharmacokinetics was largely controlled by the small size of the particles and these formulations were rapidly eliminated from the circulation.

The $t_{1/2\alpha}$ for the 15 nm ^{111}In-Bn-BCMs and ^{111}In-BCMs were not significantly different and were 0.7 ± 0.4 h and 0.3 ± 0.2 h, respectively. Similarly, the values obtained for $t_{1/2\beta}$ did not differ significantly.

3.3. Influence of BFCs and concentration of hEGF on the biodistribution of block copolymer micelles

The BCMs were largely sequestered in the liver with only a minor sequestration in the kidneys. The biodistribution of the formulations was found to depend on the density of hEGF present on the micelle surface, the BFC used for chelating ^{111}In as well as BCM size. At 48 h.p.i. the levels of labelled radioactivity remaining in all tissues was lower for mice that had received the 15 nm BCMs in comparison to those that had received the 60 nm BCMs (Figs. 5 and 6).

Fig. 5A shows the biodistribution at 48 h.p.i. of the various 60 nm BCM formulations. Tissue accumulation of the 60 nm radiolabelled BCMs depended on the density of hEGF conjugated to the surface of the BCMs. ^{111}In-5%hEGF-BCMs were cleared more rapidly from all tissues than the non-targeted ^{111}In-BCMs. Liver and spleen accumulation of the 60 nm ^{111}In-Bn-BCMs was 31.5 ± 3.6%ID/g and 15.2 ±

Table 1
Characteristics of block copolymers.

	MW-PEG	MW-PCL	PDI	CMC
MePEG-*b*-PCL	2500	1200	1.12	102 mg/L
H_2N-PEG-*b*-PCL	3000	1600	1.16	n.d.
HOOC-PEG-*b*-PCL	2500	1200	1.13	n.d.

PCL: Polycaprolactone, PEG: Poly(ethyleneglycol), CMC: critical micelle concentration. MW: molecular weights calculated from NMR spectra. n.d.: not determined. PDI: Polydispersity Index.

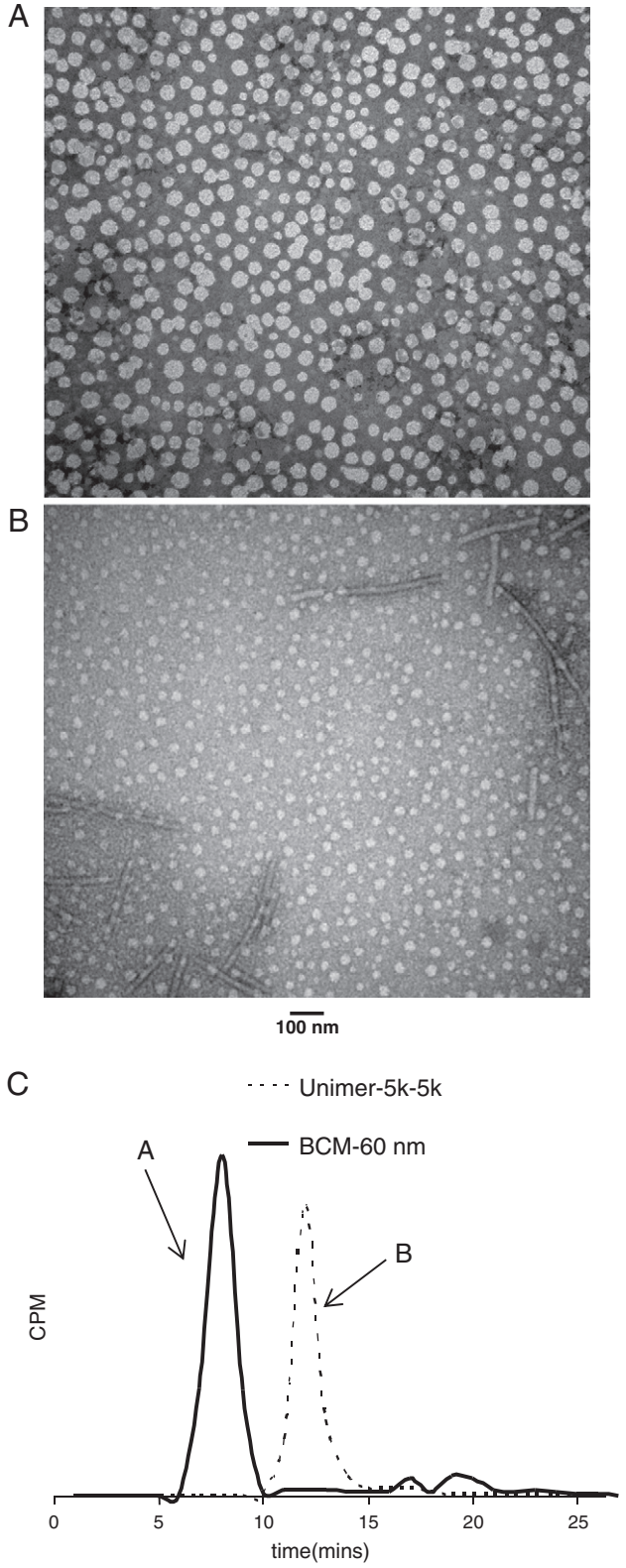

Fig. 2. A) Representative TEM image of showing the morphology of pre-formed 60 nm BCMs. B) Representative TEM image of showing the morphology of pre-formed 13 nm BCMs. C) Investigation of the extent of incorporation of radiolabelled ^{111}In-DTPA-PEG$_{5k}$-*b*-PCL$_{5k}$ into preformed BCMs using Sepharose-12 column chromatography. The chromatogram shows the incorporation of ^{111}In-DTPA-PEG$_{5k}$-*b*-PCL$_{5k}$ into pre-formed BCMs characterized by the retention time at 7 min (A) while the unincorporated unimer elutes at a later retention time of 12 min (B).

4.2%ID/g, respectively, compared ($P<0.05$) to 17.7 ± 1.0%ID/g and 1.0 ± 0.1%ID/g for the targeted ^{111}In-5%hEGF-Bn-BCMs. Tumor accumulation of ^{111}In-Bn-BCMs was 4.1 ± 0.1%ID/g compared ($P<0.05$) to 0.7 ± 0.1%ID/g for ^{111}In-5%hEGF-Bn-BCMs.

The accumulation of BCMs increased in all tissues when *p*-SCN-Bn-DTPA was used as the BFC for ^{111}In. BCMs radiolabelled via *p*-SCN-Bn-DTPA and 60 nm in diameter had a slower elimination from all tissues than the BCM formulations radiolabelled via DTPA dianhydride. Liver and spleen accumulation of ^{111}In-Bn-BCMs derivatives were significantly higher than for ^{111}In-BCMs. Similarly, elimination from the blood was slower for the ^{111}In-Bn-BCMs compared to the ^{111}In-BCMs. On the other hand, Fig. 5B shows that ^{111}In-Bn-DOTA-BCMs and ^{111}In-DOTA-BCMs yielded a similar biodistribution at 48 h.p.i. However, tumor accumulation of ^{111}In-Bn-DOTA-BCMs (2.0 ± 0.4%ID/g) was 1.6-fold higher than for ^{111}In-DOTA-BCMs (1.2 ± 0.2%ID/g).

Fig. 6 shows the biodistribution of the different 15 nm BCM formulations at 48 h.p.i. There was high uptake of the 15 nm BCM formulations in the liver and kidneys at 48 h.p.i. At this time point, the uptake of the ^{111}In-Bn-BCMs in the liver was the highest in comparison to the other formulations. Liver accumulation (and that in other tissues) decreased when hEGF-PEG$_x$-*b*-PCL$_y$ was added on the surface of the BCMs. At 48 h.p.i. liver accumulation of ^{111}In-Bn-BCMs was 6.0 ± 0.8%ID/g compared ($P<0.05$) to 3.5 ± 0.3%ID/g for ^{111}In-hEGF-Bn-BCMs. 15 nm ^{111}In-BCMs formulation had faster elimination from the circulation than the corresponding ^{111}In-Bn-BCMs/^{111}In-hEGF-Bn-BCMs. The tumor accumulation of 15 nm ^{111}In-Bn-BCMs and ^{111}In-hEGF-Bn-BCMs was comparable to ^{111}In-hEGF (Fig. 5).

^{111}In-hEGF was accumulated in the kidneys and liver with low uptake in the spleen. Kidney and liver uptake was 8.4 ± 2.4%ID/g and 9.4 ± 6.4%ID/g, respectively at 48 h.p.i. with the radiopharmaceutical being eliminated from the circulation (0.1%ID/g) at 48 h.p.i. Tumor accumulation of ^{111}In-hEGF was 0.5 ± 0.2%ID/g.

4. Discussion

Multifunctional nanotechnologies have the potential to increase the payload of therapeutic agents and decrease toxicity to non-target tissues by altering the pharmacokinetics and biodistribution of these agents. This is largely achieved by passive [8] and active targeting strategies [38]. These nanotechnologies can theoretically be more efficacious because of the high payloads of drugs and therapeutic radionuclide they can potentially carry. Additionally, their *in vivo* behaviour can easily be evaluated when they are labelled with γ- or β^+-emitting radionuclide via suitable BFC and evaluated by single photon emission computed tomography (SPECT) and positron emission tomography (PET). To achieve optimum delivery of their payload it is therefore important that formulation variables (size, morphology, charge, BFC and density of targeting group (in the case of active targeting)) that influence the delivery of nano-systems be considered. We herein report that in addition to the known effect of size of nanoparticles, the density of the targeting group (in the case of active targeting) present at the surface of the BCMs and the BFC used for complexing the radionuclide have a profound effect on the pharmacokinetics and biodistribution of the nano-delivery system.

We previously demonstrated through *in vitro* and *in vivo* experiments that the 15 and 60 nm BCMs were stable [11,32]. Specifically, the ^{111}In-PEG$_{5k}$-*b*-PCL$_{5k}$ and ^{111}In-PEG$_{2.5k}$-*b*-PCL$_{1.2k}$ micelles were found to be stable *in vitro* in mouse plasma over a 72 h period with minimal *in vivo* transchelation to transferrin [11,32]. Liu et al. [36] found that after i.v. administration of 60 nm BCMs (CMC of MePEG$_{5k}$-*b*-PCL$_{5k}$ = 38 mg/mL) at 250 mg/kg (94 times above CMC, assuming blood is 7% of body weight) or 2 mg/kg (1.4 times below CMC), there was respectively, 74% or 55% intact BCMs after 24 h.p.i. Hoang et al. [32] also showed a significant difference in pharmacokinetics and biodistribution when ^{111}In-BCMs were injected at concentrations above

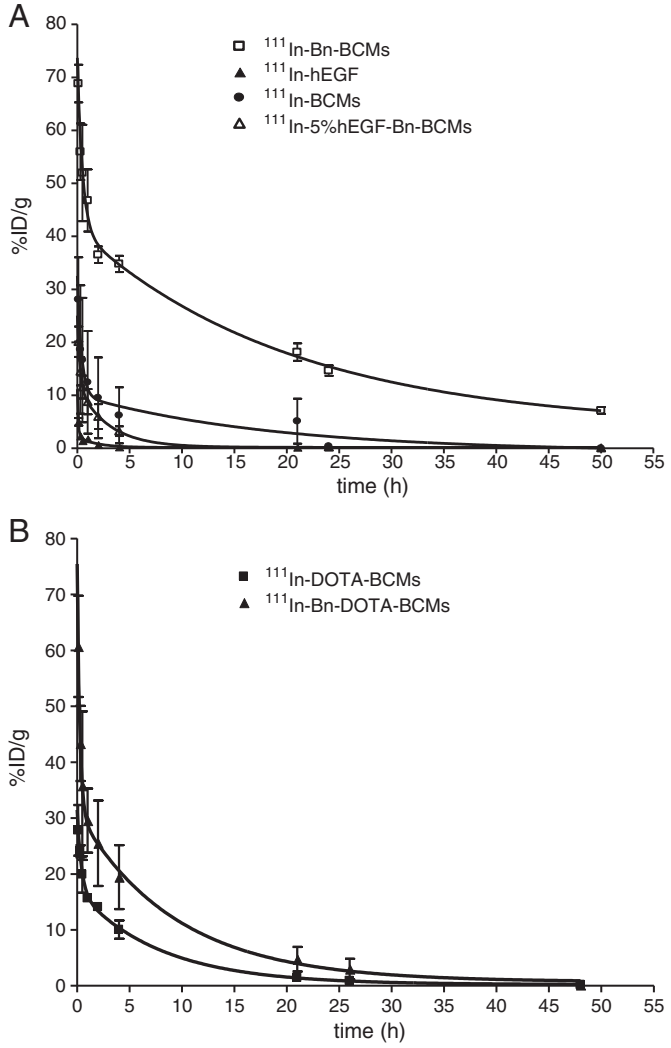

Fig. 3. A: Blood clearance curve of 60 nm ^{111}In-labelled BCMs in athymic CD-1 nude mice ($n \geq 3$) bearing s.c. MDA-MB-468 human breast cancer xenografts. BCMs were labelled with ^{111}In via *p*-SCN-Bn-DTPA (non-targeted, ^{111}In-Bn-BCMs) or DTPA bis-anhydride (non-targeted, ^{111}In-BCMs). Blood clearance curve of BCMs containing 5 mol% hEGF targeted BCMs (^{111}In-5%hEGF-Bn-BCMs) is also shown. ^{111}In-hEGF is also shown for comparison. Blood radioactivity concentrations were fitted into a two-compartment pharmacokinetic model. Data expressed as % injected dose per gram (%ID/g) ± standard deviation. B: Blood clearance curve of 60 nm BCMs in athymic CD-1 nude mice ($n \geq 3$) bearing s.c. MDA-MB-468 human breast cancer xenografts. BCMs were labelled with ^{111}In via *p*-SCN-Bn-DOTA (non-targeted, ^{111}In-Bn-DOTA-BCMs) or NHS-DOTA (non-targeted, ^{111}In-DOTA-BCMs). Blood radioactivity concentrations were fitted into a two-compartment pharmacokinetic model. Data expressed as % injected dose per gram (%ID/g) ± standard deviation.

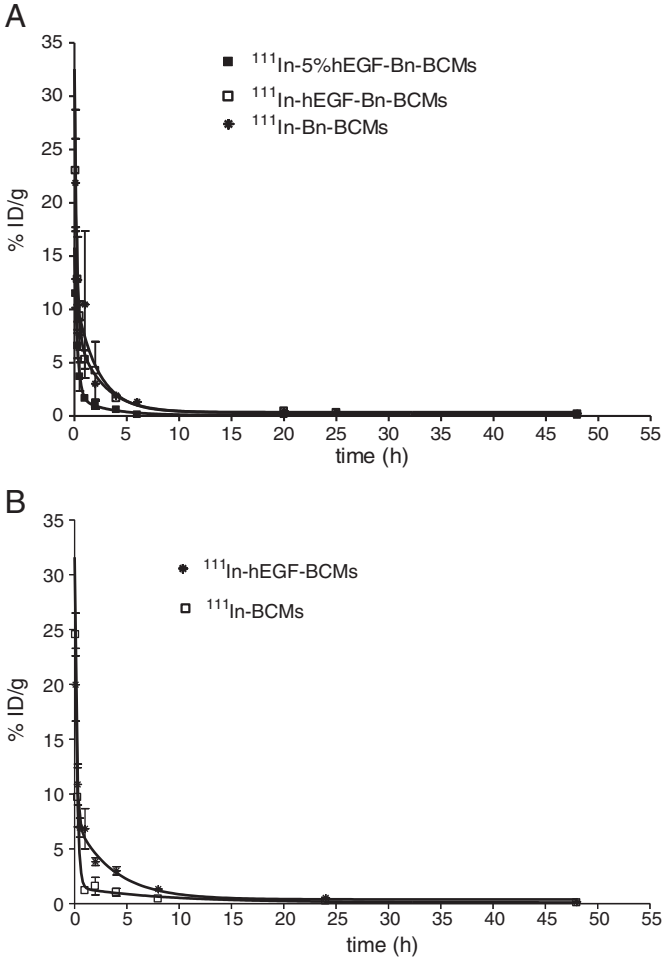

Fig. 4. A: Blood clearance curve of 15 nm BCMs in athymic CD-1 nude mice ($n \geq 3$) bearing s.c. MDA-MB-468 human breast cancer xenografts. BCMs were labelled with ^{111}In via *p*-SCN-Bn-DTPA (non-targeted, ^{111}In-Bn-BCMs or 1 mol% hEGF ^{111}In-Bn-hEGF-BCMs or 5 mol% hEGF, ^{111}In-5%hEGF-Bn-BCMs). Blood radioactivity concentrations were fitted into a two-compartment pharmacokinetic model. Data expressed as % injected dose per gram (%ID/g) ± standard deviation. B: Blood clearance curve of 15 nm BCMs in athymic CD-1 nude mice ($n \geq 3$) bearing s.c. MDA-MB-468 human breast cancer xenografts. BCMs were labelled with ^{111}In using DTPA dianhydride (non-targeted, ^{111}In-BCMs or 5 mol% hEGF ^{111}In-hEGF-BCMs). Blood radioactivity concentrations were fitted into a two-compartment pharmacokinetic model. Data expressed as % injected dose per gram (%ID/g) ± standard deviation.

and below the CMC. Similar to the 60 nm BCMs the 15 nm BCMs were injected (250 mg/kg) at a concentration 33-fold above CMC (108 mg/L).

Contrary to the previously held notion that the BFC agent employed only influences the pharmacokinetics of small molecules but not macromolecules or nano-delivery systems, an increasing number of studies have recently shown that the BFC exerts similar effects when conjugated to biomacromolecules [29,31,39]. In a mouse model of HER-2 over-expressing breast cancer, Tomalchev et al. [31] showed a significant difference in tissue biodistribution and HER-2 targeting efficiency for anti-HER-2 affibodies (6 KDa) when *p*-NH_2-Bn-DOTA or N-[(R)-2-amino-3-(*p*-aminophenyl) propyl]-trans-(S, S)-cyclohexane-1,2-diamine-N,N,N′,N′′,N′′-pentaacetic acid (*p*-NH_2-Bn-CHX-A′′-DTPA) were used as the BFC for labelling with ^{114m}In. Tumor, heart, spleen, blood, liver and lung uptake of ^{114m}In-labelled Bn-CHX-A"-DTPA-affibody were higher than for ^{114m}In-labelled Bn-DOTA-affibody. They concluded that the ^{114m}In-labelled Bn-CHX-A"-DTPA-affibody was better at targeting HER-2 overexpression *in vivo* compared to the ^{114m}In-labelled Bn-DOTA-affibody

Table 2
Pharmacokinetic parameters of the 60 nm ^{111}In-labelled Bn-BCMs, BCMs, 5%hEGF-Bn-BCMs, DOTA-BCMs, Bn-DOTA-BCMs and hEGF.

BCMs	$t_{1/2\alpha}$ [h]	$t_{1/2\beta}$ [h]	CL [mL/h]	AUC [%ID/mL × h]	V_1 [mL]
Bn-BCMs*‡	0.6 ± 0.5	24.8 ± 7.1	0.07 ± 0.02	15.6 ± 5.3	1.5 ± 0.3
BCMs*	0.5 ± 0.2	11.8 ± 3.3	0.3 ± 0.1	3.4 ± 1.4	3.1 ± 0.7
Bn-DOTA-BCMs†	0.2 ± 0.1	8.7 ± 1.7	0.3 ± 0.1	4.2 ± 1.1	1.5 ± 0.1
DOTA-BCMs†	1.1 ± 1.1	14.7 ± 10.4	0.5 ± 0.0	2.2 ± 0.1	3.7 ± 0.1
5%hEGF-Bn-BCMs‡	1.1 ± 1.0	15.0 ± 9.1	1.1 ± 0.1	6.6 ± 0.9	5.1 ± 1.5
hEGF	0.2 ± 0.1	25.5 ± 7.6	3.3 ± 0.9	1.9 ± 0.45	18.4 ± 4.1

60 nm Block copolymer micelles (BCMs) labelled with ^{111}In via p-SCN-Bn-DTPA (Bn-BCMs), DTPA anhydride (BCMs), p-SCN-Bn-DOTA (Bn-DOTA-BCMs) or DOTA (DOTA-BCMs). BCMs containing 5 mol% hEGF (5%hEGF-Bn-BCMs) and ^{111}In-labelled hEGF. Bn: benzyl. Statistical significance ($P<0.05$) for * (^{111}In-Bn-BCMs vs ^{111}In-BCMs), ‡ (^{111}In-Bn-BCMs vs ^{111}In-5%hEGF-Bn-BCMs) and † (^{111}In-Bn-DOTA-BCMs vs ^{111}In-DOTA-BCMs for CL and AUC).

Table 3
Pharmacokinetics parameters of the 15 nm BCMs, hEGF-BCMs and 5%hEGF-BCMs in CD-1 nude mice bearing MDA-MB-468 breast cancer xenografts.

BCMs	$t_{1/2\alpha}$ [h]	$t_{1/2\beta}$ [h]	CL [mL/h]	AUC [%ID/mL × h]	V_1 [mL]
Bn-BCMs	0.7 ± 0.4	26.4 ± 13.4	1.1 ± 0.2	0.9 ± 0.1	6.1 ± 2.6
BCMs	0.3 ± 0.2	23.6 ± 14.1	1.3 ± 0.1	1.4 ± 1.5	2.9 ± 1.2
hEGF-Bn-BCMs	0.3 ± 0.0	12.6 ± 1.7	1.6 ± 0.0	0.6 ± 0.0	4.1 ± 1.0
hEGF-BCMs	0.5 ± 0.2	16.1 ± 6.4	6.7 ± 0.1	1.5 ± 0.3	5.6 ± 0.3
5%hEGF-BCMs	0.2 ± 0.0	23.8 ± 6.5	2.5 ± 0.2	0.4 ± 0.0	6.6 ± 1.0

15 nm Block copolymer micelles (BCMs) labelled with ^{111}In via p-SCN-Bn-DTPA (Bn-BCMs) or DTPA anhydride (BCMs). ^{111}In-labelled BCMs containing 1 mol% hEGF (hEGF-Bn-BCMs) or 5 mol% hEGF (5%hEGF-Bn-BCMs) Bn: benzyl.

bioconjugate. In another study, Sabbah et al. [40] compared the biodistribution and tumor targeting of an ^{111}In-Bn-CHX-A′′-DTPA-antiferritin monoclonal antibody (mAb) with ^{111}In-Bn-DOTA-antiferritin mAb or ^{111}In-Bn-DTPA-antiferritin mAb in mice. The three immunoconjugates showed significant differences in liver, blood, bone and tumor uptake. Notably, in human pancreatic adenocarcinoma CAPAN-1 bearing mice, tumor uptake of ^{111}In-Bn-DTPA-antiferritin mAb was more than 2-fold higher than for ^{111}In-Bn-DOTA-antiferritin mAb even though there was no difference in their immunoreactivity *in vitro*. Even though the BFCs used in this study form very stable chelates with ^{111}In, disaggregation of the micelles into unimers *in vivo* is expected over a long period of time (but not over the course of your experiments). Similar to the above studies, we have also found significant differences in the pharmacokinetics and biodistribution when BCMs were labelled with ^{111}In via DTPA bis-anhydride, *p*-SCN-Bn-DTPA, NHS-DOTA or *p*-SCN-Bn-DOTA as BFC. Blood pharmacokinetics and tissue clearance was slower for ^{111}In-Bn-BCMs than for the other chelators and the corresponding tumor accumulation was higher. Some authors have reported that *in vitro* and *in vivo* differences observed between ^{111}In-labelled Bn-DTPA-biomolecules and ^{111}In-labelled DTPA-biomolecules are due to the inherent enhanced stability of the former resulting from the difference in the denticity. As shown in Fig. 1*p*-SCN-Bn-DTPA and *p*-SCN-Bn-DOTA preserve the octa-dentate ^{111}In–chelate complex when conjugated to the polymers compared to DTPA bis-anhydride and NHS-DOTA which yield a hepta-dentate ^{111}In–chelate complex [41,42]. Our *in vitro* studies in plasma did not show significant differences in stability between ^{111}In-labelled DTPA-BCMs/DOTA-BCMs and Bn-DTPA-BCMs/Bn-DOTA-BCMs despite the fact that octa-dentate complexes of ^{111}In are more thermodynamically stable [43]. If the observed differences in the *in vivo* biodistribution were due to the conjugation and complexation chemistry employed (i.e. C-functionalization resulting in an octadentate complex, in the case of *p*-SCN-Bn-DTPA or N-functionalization producing a heptadentate complex in the case of DTPA dianhydride) there would be insignificant differences in the biodistribution and pharmacokinetics of biomolecules labelled via *p*-SCN-Bn-DOTA or *p*-SCN-Bn-DTPA which both yield stable octadentate ^{111}In–chelate complexes. As reported in the present study and by many authors [29,31,39,40] these differences indicate that conjugation and complexation do not fully account for the observed differences. Another factor that can contribute to the difference in blood elimination and biodistribution is the lipophilicity of the complex. Lipophilic complexes (^{111}In-Bn-BCMs/^{111}In-Bn-DOTA-BCMs; due to the lipophilic benzyl-group) tend to have slower blood elimination due to their increased association with plasma lipoproteins. Our results show significant differences for DTPA and DOTA derivatives confirming earlier reports observed for biomolecules [31,40]. The AUC and CL of the 60 nm ^{111}In-labelled BCMs conjugated via *p*-SCN-Bn-DTPA were 3.7-fold larger and 4.2-fold slower, respectively, than ^{111}In-labelled BCMs conjugated via *p*-SCN-Bn-DOTA. As well uptake in the MDA-MB-468 tumor was 2-fold higher for the former. These results show that *p*-SCN-Bn-DTPA enables a superior passive targeting effect to be achieved in comparison to the DTPA anhydride or DOTA/*p*-SCN-Bn-DOTA conjugated BCMs. A detailed understanding of these differences requires further investigation.

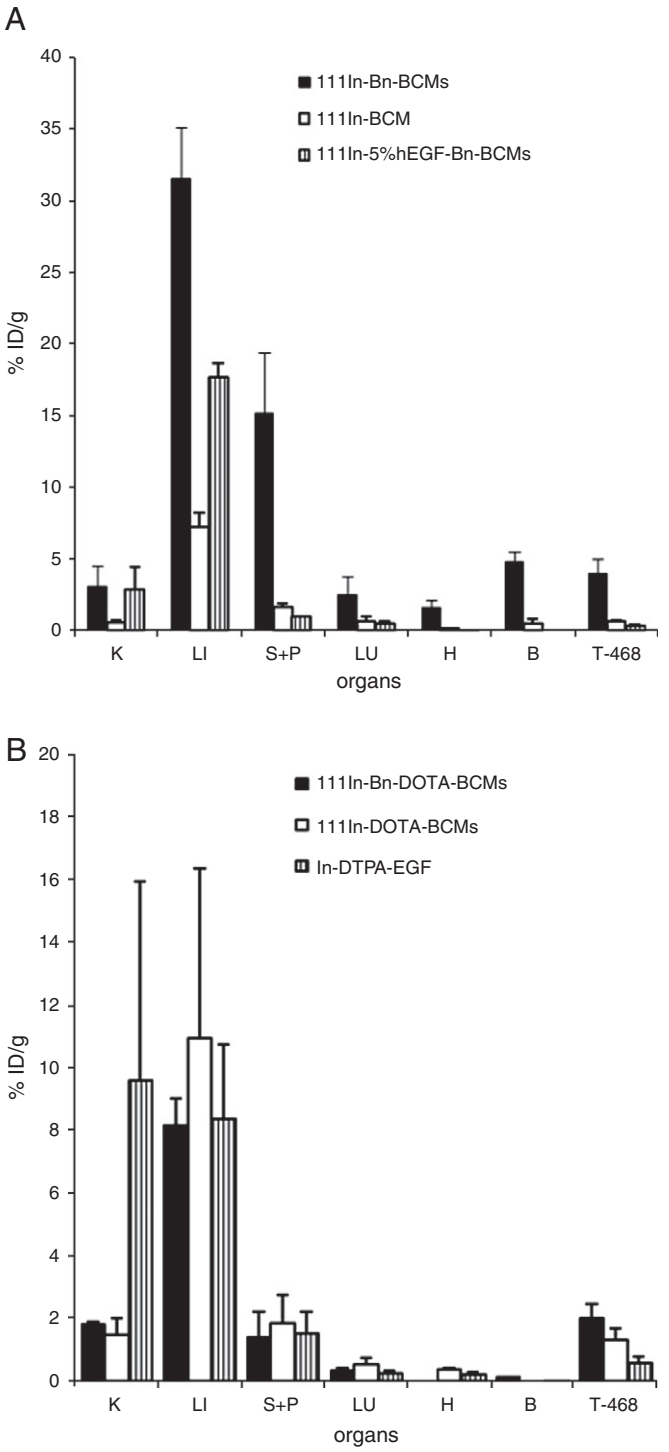

Fig. 5. A: Biodistribution at 48 h.p.i. of 60 nm non-targeted ^{111}In-Bn-BCMs and ^{111}In-BCMs or hEGF-targeted ^{111}In-5%hEGF-Bn-BCMs (5 mol% hEGF) in athymic CD-1 nude mice (n ≥ 3) bearing s.c. MDA-MB-468 human breast cancer xenografts. Data expressed as % injected dose per gram (%ID/g) ± standard deviation. Where T-MDA-MB-468 is uptake in MDA-MB-468 tumor. B: Biodistribution at 48 h.p.i. of 60 nm non-targeted ^{111}In-Bn-DOTA-BCMs and ^{111}In-DOTA-BCMs or ^{111}In-hEGF in athymic CD-1 nude mice (n ≥ 3) bearing s.c. MDA-MB-468 human breast cancer xenografts at 48 h.p.i. Data expressed as % injected dose per gram (%ID/g) ± standard deviation. Where K: kidneys, LI: liver, S + P: spleen + pancreas, LU: lungs, H: heart, B: blood and T-468 is uptake in MDA-MB-468 tumor.

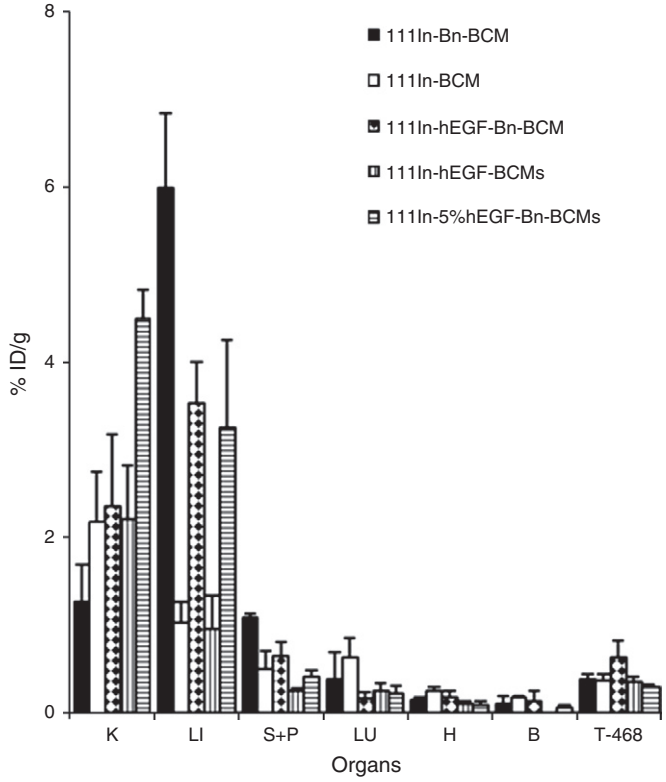

Fig. 6. Biodistribution of 15 nm non-targeted ^{111}In-Bn-BCMs and ^{111}In-BCMs or hEGF targeted ^{111}In-hEGF-Bn-BCMs (1 mol% hEGF), ^{111}In-5%hEGF-Bn-BCMs (5 mol% hEGF) or ^{111}In-hEGF-BCMs in athymic CD-1 nude mice bearing ($n \geq 3$) s.c. MDA-MB-468 human breast cancer xenografts at 48 h.p.i. Data expressed as % injected dose per gram (%ID/g) ± standard deviation. Where K: kidneys, LI: liver, S + P: spleen + pancreas, LU: lungs, H: heart, B: blood and T-468 is uptake in MDA-MB-468 tumor.

When BCMs are functionalized with moieties that target specific receptors overexpressed on the cell surface, these moieties can have an effect on the pharmacokinetics and biodistribution of the delivery system, and indeed are expected to influence tumor uptake. In studies where immunoliposomes were functionalized with IgG mAb, increased recognition by Fc receptors in the liver led to a faster clearance of these nanoparticles from the circulation [18,44]. The density of the targeting ligand on the surface of nano-delivery systems required to achieve optimal tumor targeting varies [18,45–47]. For example, authors have shown that the uptake in HER-2 overexpressing SK-BR-3 cells varies with the density of anti-HER-2 Fab′ on the surface of immunoliposomes and this plateaus at 30–40 Fab′ per immunoliposome, with decreased binding on further addition of anti-HER-2 Fab′ [46,47]. Using 30–40 Fab′ per immunoliposome, the pharmacokinetics were equivalent to that of non-targeted liposomes [17,48]. However, no information was provided comparing the pharmacokinetics and tumor uptake of immunoliposomes with different anti-HER-2 Fab′ densities. The present study shows that the density of hEGF on the surface of BCMs influences their *in vivo* pharmacokinetics and biodistribution. At a concentration of 5 mol% hEGF, ^{111}In-hEGF-Bn-BCM exhibited significantly faster elimination from the circulation than the non-targeted ^{111}In-Bn-BCMs. The $t_{1/2\beta}$, CL, AUC, and V_1 of the ^{111}In-Bn-BCMs were significantly different from the values obtained for ^{111}In-hEGF-Bn-BCM. We previously showed that when BCMs were formulated with 0.2 mol% hEGF-PEG-*b*-PCL the pharmacokinetics and biodistribution did not significantly differ from the non-targeted BCMs [12]. The liver has an abundance of EGF receptors and the recognition of these receptors by EGF functionalized BCMs may enhance opsonisation and clearance of the particles similar to the effect observed for immunoliposomes modified with IgG antibodies.

5. Conclusion

The results of this study highlight some key parameters that must be considered in order to achieve optimal pharmacokinetics and biodistribution of BCMs as multifunctional nano-delivery systems. Increasing the density of the targeting moiety on the surface of the targeted nano-delivery system is often considered a strategy to maximize intracellular delivery. However caution must be taken to ensure that this increase will not lead to a deleterious effect by promoting rapid elimination and sequestration by normal tissues and consequently lower tumor accumulation. Radiolabelling of these systems provides an opportunity for facile measurement of concentrations in the blood and tissues but careful selection of BFC for complexing the radiometal should not only be based on the stability of the resulting chelate–metal complex but also on its influence on the pharmacokinetics and biodistribution of the resulting nano-delivery system. In this study *p*-SCN-Bn-DTPA satisfies these criteria and thus, we plan on using this BFC in the formulation of BCMs for further *in vivo* studies.

Acknowledgments

This study was supported by a grant from the Canadian Institutes of Health Research to C.A. and R.M.R (Grant #483549). H.F. is grateful to the Ontario Ministry of Innovation and Research for a post-doctoral fellowship. The authors also thank Drs. Zhongli Cai and Changhai Lu for technical assistance.

References

[1] S.E. Krown, D.W. Northfelt, D. Osoba, J.S. Stewart, Use of liposomal anthracyclines in Kaposi's sarcoma, Semin. Oncol. 31 (Suppl. 13) (2004) 36–52.
[2] A.C. Wolff, Liposomal anthracyclines and new treatment approaches for breast cancer, Oncologist 8 (Suppl. 2) (2003) 25–30.
[3] P. Chu, S. Sadullah, The current role of amphotericin B lipid complex in managing systemic fungal infections, Curr. Med. Res. Opin. 25 (2009) 3011–3020.
[4] S. Danson, D. Ferry, V. Alakhov, J. Margison, D. Kerr, D. Jowle, M. Brampton, G. Halbert, M. Ranson, Phase I dose escalation and pharmacokinetic study of pluronic polymer-bound doxorubicin (SP 1049C) in patients with advanced cancer, Br. J. Cancer 90 (2004) 2085–2091.
[5] J. Homsi, G.R. Simon, C.R. Garrett, G. Springett, R. De Conti, A.A. Chiappori, P.N. Munster, M.K. Burton, S. Stromatt, C. Allievi, P. Angiuli, A. Eisenfeld, D.M. Sullivan, A.I. Daud, Phase I trial of poly-L-glutamate camptothecin (CT-2106) administered weekly in patients with advanced solid malignancies, Clin. Cancer Res. 13 (2007) 5855–5861.
[6] Y. Matsumura, M. Gotoh, K. Muro, Y. Yamada, K. Shirao, Y. Shimada, M. Okuwa, S. Matsumoto, Y. Miyata, H. Ohkura, K. Chin, S. Baba, T. Yamao, A. Kannami, Y. Takamatsu, K. Ito, K. Takahashi, Phase I and pharmacokinetic study of MCC-465, a doxorubicin (DXR) encapsulated in PEG immunoliposome, in patients with metastatic stomach cancer, Ann. Oncol. 15 (2004) 517–525.
[7] Y. Matsumura, T. Hamaguchi, T. Ura, K. Muro, Y. Yamada, Y. Shimada, K. Shirao, T. Okusaka, H. Ueno, M. Ikeda, N. Watanabe, Phase I clinical trial and pharmacokinetic evaluation of NK911, a micelle-encapsulated doxorubicin, Br. J. Cancer 91 (2004) 1775–1781.
[8] V.P. Torchilin, Recent advances with liposomes as pharmaceutical carriers, Nat. Rev. 4 (2005) 145–160.
[9] V.P. Torchilin, Multifunctional nanocarriers, Adv. Drug. Deliv. Rev. 58 (2006) 1532–1555.
[10] M. Ferrari, Cancer nanotechnology: opportunities and challenges, Nat. Rev. Cancer 5 (2005) 161–171.
[11] H. Fonge, H. Lee, R.M. Reilly, C. Allen, Multifunctional block copolymer micelles for the delivery of ^{111}In to EGFR-positive breast cancer cells for targeted Auger electron radiotherapy, Mol. Pharm. 7 (2010) 177–186.
[12] H. Lee, B. Hoang, H. Fonge, R.M. Reilly, C. Allen, *In vivo* distribution of polymeric nanoparticles at the whole-body, tumor, and cellular levels, Pharm. Res. 27 (2010) 2343–2355.
[13] J. Zheng, C. Allen, S. Serra, D. Vines, M. Charron, D.A. Jaffray, Liposome contrast agent for CT-based detection and localization of neoplastic and inflammatory lesions in rabbits: validation with FDG-PET and histology, Contrast Media Mol. Imaging 5 (2010) 147–154.
[14] J. Zheng, D. Jaffray, C. Allen, Quantitative CT imaging of the spatial and temporal distribution of liposomes in a rabbit tumor model, Mol. Pharm. 6 (2009) 571–580.
[15] A.S. Mikhail, C. Allen, Block copolymer micelles for delivery of cancer therapy: transport at the whole body, tissue and cellular levels, J. Control. Release 138 (2009) 214–223.
[16] D.B. Kirpotin, D.C. Drummond, Y. Shao, M.R. Shalaby, K. Hong, U.B. Nielsen, J.D. Marks, C.C. Benz, J.W. Park, Antibody targeting of long-circulating lipidic

nanoparticles does not increase tumor localization but does increase internalization in animal models, Cancer Res. 66 (2006) 6732–6740.
[17] C. Mamot, D.C. Drummond, C.O. Noble, V. Kallab, Z. Guo, K. Hong, D.B. Kirpotin, J.W. Park, Epidermal growth factor receptor-targeted immunoliposomes significantly enhance the efficacy of multiple anticancer drugs *in vivo*, Cancer Res. 65 (2005) 11631–11638.
[18] K. Maruyama, N. Takahashi, T. Tagawa, K. Nagaike, M. Iwatsuru, Immunoliposomes bearing polyethyleneglycol-coupled Fab' fragment show prolonged circulation time and high extravasation into targeted solid tumors *in vivo*, FEBS Lett. 413 (1997) 177–180.
[19] K.M. McNeeley, A. Annapragada, R.V. Bellamkonda, Decreased circulation time offsets increased efficacy of PEGylated nanocarriers targeting folate receptors of glioma, Nanotechnology 18 (2007) 1–11.
[20] P. Sapra, T.M. Allen, Ligand-targeted liposomal anticancer drugs, Prog. Lipid Res. 42 (2003) 439–462.
[21] H. Maeda, Tumor-selective delivery of macromolecular drugs via the EPR effect: background and future prospects, Bioconjug. Chem. 21 (2010) 797–802.
[22] F. Alexis, E. Pridgen, L.K. Molnar, O.C. Farokhzad, Factors affecting the clearance and biodistribution of polymeric nanoparticles, Mol. Pharm. 5 (2008) 505–515.
[23] J. Fang, H. Nakamura, H. Maeda, The EPR effect: unique features of tumor blood vessels for drug delivery, factors involved, and limitations and augmentation of the effect, Adv. Drug Deliv. Rev. 63 (2011) 136–151.
[24] R. Gref, Y. Minamitake, M.T. Peracchia, V. Trubetskoy, V. Torchilin, R. Langer, Biodegradable long-circulating polymeric nanospheres, Science 263 (1994) 1600–1603.
[25] S.M. Moghimi, A.C. Hunter, J.C. Murray, Long-circulating and target-specific nanoparticles: theory to practice, Pharmacol. Rev. 53 (2001) 283–318.
[26] J.E. Riviere, Pharmacokinetics of nanomaterials: an overview of carbon nanotubes, fullerenes and quantum dots, Wiley Interdiscip. Rev. Nanomed. Nanobiotechnol. 1 (2009) 26–34.
[27] T.A. ElBayoumi, V.P. Torchilin, Tumor-targeted nanomedicines: enhanced antitumor efficacy *in vivo* of doxorubicin-loaded, long-circulating liposomes modified with cancer-specific monoclonal antibody, Clin. Cancer Res. 15 (2009) 1973–1980.
[28] H. Fonge, L.X. Jin, J. Cleynhens, G. Bormans, A. Verbruggen, Tc-99m-tricarbonyl labelled agents for cell labeling: development, biodistribution in normal mice and preliminary in vitro evaluation, Bioorg. Med. Chem. 18 (2010) 396–402.
[29] S. Chakraborty, S. Liu, (99m)Tc and (111)In-labeling of small biomolecules: bifunctional chelators and related coordination chemistry, Curr. Top. Med. Chem. 10 (2010) 1113–1134.
[30] G. Liu, D.J. Hnatowich, Labeling biomolecules with radiorhenium: a review of the bifunctional chelators, Anticancer Agents Med. Chem. 7 (2007) 367–377.
[31] V. Tolmachev, H. Wallberg, K. Andersson, A. Wennborg, H. Lundqvist, A. Orlova, The influence of Bz-DOTA and CHX-A"-DTPA on the biodistribution of ABD-fused anti-HER2 affibody molecules: implications for ^{114m}In-mediated targeting therapy, Eur. J. Nucl. Med. Mol. Imaging 36 (2009) 1460–1468.
[32] B. Hoang, H. Lee, R. Reilly, C. Allen, Non-invasive monitoring of the fate of ^{111}In-labelled block copolymer micelles by high resolution and high sensitivity Micro-SPECT/CT imaging, Mol. Pharm. 6 (2009) 581–592.
[33] F. Zeng, C. Allen, Synthesis of carboxy-functionalized heterobifunctional poly (ethylene glycol) by a thiol-anionic polymerization method, Macromolecules 39 (2006) 6391–6398.
[34] F. Zeng, H. Lee, C. Allen, Epidermal growth factor-conjugated poly(ethylene glycol)-block-poly(delta-valerolactone) copolymer micelles for targeted delivery of chemotherapeutics, Bioconjug. Chem. 17 (2006) 399–409.
[35] X. Zhang, J.K. Jackson, H.M. Burt, Determination of surfactant critical micelle concentration by a novel fluorescence depolarization technique, J. Biochem. Biophys. Methods 31 (1996) 145–150.
[36] J. Liu, F. Zeng, C. Allen, *In vivo* fate of unimers and micelles of a poly(ethylene glycol)-block-poly(caprolactone) copolymer in mice following intravenous administration, Eur. J. Pharm. Biopharm. 65 (2007) 309–319.
[37] J. Filmus, M.N. Pollak, R. Cailleau, R.N. Buick, MDA-468, a human breast cancer cell line with a high number of epidermal growth factor (EGF) receptors, has an amplified EGF receptor gene and is growth inhibited by EGF, Biochem. Biophys. Res. Commun. 128 (1985) 898–905.
[38] R.E. Kontermann, Immunoliposomes for cancer therapy, Curr. Opin. Mol. Ther. 8 (2006) 39–45.
[39] T. Ekblad, A. Orlova, J. Feldwisch, A. Wennborg, A.E. Karlstrom, V. Tolmachev, Positioning of ^{99m}Tc-chelators influences radiolabeling, stability and biodistribution of affibody molecules, Bioorg. Med. Chem. Lett. 19 (2009) 3912–3914.
[40] E.N. Sabbah, J. Kadouche, D. Ellison, C. Finucane, D. Decaudin, S.J. Mather, In vitro and *in vivo* comparison of DTPA- and DOTA-conjugated antiferritin monoclonal antibody for imaging and therapy of pancreatic cancer, Nucl. Med. Biol. 34 (2007) 293–304.
[41] A.L. Sundberg, A. Orlova, A. Bruskin, L. Gedda, J. Carlsson, E. Blomquist, H. Lundqvist, V. Tolmachev, ^{111}In-Bz-DTPA-hEGF: preparation and in vitro characterization of a potential anti-glioblastoma targeting agent, Cancer Biother. Radiopharm. 18 (2003) 643–654.
[42] R.W. Kozak, A. Raubitschek, S. Mirzadeh, M.W. Brechbiel, R.P. Junghans, O.A. Gansow, T.A. Waldmann, Nature of the bifunctional chelating agent used for radioimmunotherapy with yttrium-90 monoclonal antibodies: critical factors in determining *in vivo* survival and organ toxicity, Cancer Res. 49 (1989) 2639–2644.
[43] H.R. Maecke, A. Riesen, W. Ritter, The molecular structure of indium-DTPA, J. Nucl. Med. 30 (1989) 1235–1239.
[44] B. Gupta, T.S. Levchenko, D.A. Mongayt, V.P. Torchilin, Monoclonal antibody 2C5-mediated binding of liposomes to brain tumor cells in vitro and in subcutaneous tumor model *in vivo*, J. Drug Target 13 (2005) 337–343.
[45] J.A. Kamps, G.L. Scherphof, Receptor versus non-receptor mediated clearance of liposomes, Adv. Drug Deliv. Rev. 32 (1998) 81–97.
[46] J.W. Park, K. Hong, D.B. Kirpotin, O. Meyer, D. Papahadjopoulos, C.C. Benz, Anti-HER2 immunoliposomes for targeted therapy of human tumors, Cancer Lett. 118 (1997) 153–160.
[47] D. Kirpotin, J.W. Park, K. Hong, S. Zalipsky, W.L. Li, P. Carter, C.C. Benz, D. Papahadjopoulos, Sterically stabilized anti-HER2 immunoliposomes: design and targeting to human breast cancer cells in vitro, Biochemistry 36 (1997) 66–75.
[48] J.W. Park, K. Hong, D.B. Kirpotin, G. Colbern, R. Shalaby, J. Baselga, Y. Shao, U.B. Nielsen, J.D. Marks, D. Moore, D. Papahadjopoulos, C.C. Benz, Anti-HER2 immunoliposomes: enhanced efficacy attributable to targeted delivery, Clin. Cancer Res. 8 (2002) 1172–1181.